ELSEVIER

International Journal of Heat and Fluid Flow 19 (1998) 482–491

International Journal of HEAT AND FLUID FLOW

DNS of turbulent heat transfer in channel flow with low to medium-high Prandtl number fluid

Hiroshi Kawamura [a,*], Kouichi Ohsaka [a], Hiroyuki Abe [a], Kiyoshi Yamamoto [b]

[a] *Department of Mechanical Engineering, Science University of Tokyo, Noda-shi, Chiba-ken 278, Japan*
[b] *National Aerospace Laboratory, Choufu-shi, Tokyo 182, Japan*

Abstract

The direct numerical simulation (DNS) of the turbulent heat transfer for various Prandtl numbers ranging from 0.025 to 5 are performed to obtain statistical quantities such as turbulent heat flux, temperature variance and their budget terms. The configuration is the fully developed channel flow with uniform heating from both walls. The Reynolds number based on the friction velocity and the channel half width is 180. Turbulent Prandtl number Pr_t is independent of Pr except for $Pr < 0.1$. The time constant ratio is also obtained and its dependence on the Pr is examined. Budget of wall-normal heat flux shows that the temperature-pressure gradient correlation (TPG) is dominant as the destruction term for a larger Pr while the dissipation is for a smaller Pr. The two become comparable at $Pr = 0.2$ for the present Reynolds number. The budget terms in the transport equation for the turbulent heat flux are visualized and the influence of Pr is discussed.

Keywords: DNS; Turbulent heat transfer; Prandtl number; Turbulent Prandtl number; Time constant ratio; Channel flow

Notation

a	thermal diffusivity
b_j, c_j, d_i	coefficient of expansion
c_p	specific heat at constant pressure
k	turbulence energy
Nu	Nusselt number
P	pressure
p	pressure fluctuation
Pr	molecular Prandtl number
Pr_t	turbulent Prandtl number
P_θ	production term of temperature variance
q_w	wall heat flux
q_{total}	total heat flux
R	time constant ratio
Re_τ	Reynolds number $= u_\tau \delta / v$
Re_m	Reynolds number $= 2Re_\tau \langle U^+ \rangle$
t	time
T	temperature
u_i, u, v, w	velocity fluctuation
u_τ	friction velocity $= \sqrt{\tau_w/\rho}$
U_i	statistically averaged velocity
x_1, x	streamwise direction
x_2, y	wall-normal direction
x_3, z	spanwise direction

Greek

α	heat transfer coefficient
δ	channel half width
ε	dissipation term of turbulent energy
ε_θ	dissipation term of temperature variance
$\varepsilon_{i\theta}$	dissipation term of turbulent heat flux
θ	temperature fluctuation
θ_τ	friction temperature $= \overline{q}_w / \rho c_p u_\tau$
Θ	transformed temperature
v	kinematic viscosity
ρ	density
τ_w	statistically averaged wall shear stress
$\phi_{i\theta}$	temperature pressure-gradient correlation

Superscripts

$(\ )^*$	normalized by δ
$(\ )^+$	normalized by u_τ, v and θ_τ
$\overline{(\ )}$	statistical averaged
$(\sim)$	instantaneous value
$\langle\ \rangle$	averaged over the channel section

1. Introduction

Several direct numerical simulations (DNS's) of the turbulent heat transfer in a channel flow were performed. Turbulent heat transfer is characterized not only by the Reynolds number (Re) but also by the Prandtl number (Pr) of the fluids. Kim and Moin (1989) made simulations for Prandtl numbers $Pr = 0.1$, 0.71 and 2 with $Re_\tau = 180$. They assumed a constant volumetric heating with a uniform wall temperature. Profiles of the mean temperature, temperature variance and turbulent heat flux were obtained; but detailed budget of the transport equations for those quantities was not reported. Later, Lyons

* Corresponding author. E-mail: kawa@muraapl.me.moda.sut.ac.jp.

0142-727X/98/$ – see front matter
PII: S0142-727X(98)10026-7

et al. (1991) made the similar DNS for $Pr = 1.0$ with a lower Reynolds number of $Re_\tau = 150$. Both walls of their channel were kept at different temperatures. Kasagi et al. (1992) and Kasagi and Ohtsubo (1993) performed DNS for $Pr = 0.025$ and 0.71 with $Re_\tau = 150$. The averaged heat flux $\bar{q}_w$ was uniform over both the heating walls; but instantaneous heat flux may vary with respect to time and position. They obtained the budget for the temperature variance and the turbulent heat fluxes. The turbulent Prandtl number and the time constant ratio for the scalar transport were also examined. In summary the DNS's were performed for the heat transfer of a liquid metal ($Pr = 0.025$) and gases ($Pr \approx 1$) up to now; however, the heat transfer of water ($Pr = 5$–7) has not yet been done. This is because the increase of the Prandtl number requires a larger mesh number.

The numerical method adopted in all the calculations was the spectral method, which is more accurate than the finite difference method, but it is less flexible in application to a complex geometry. The present author's group examined the consistency between the analytical and numerical differential operations. Kawamura (1995) showed that the DNS could be performed with a sufficiently high accuracy by using the finite difference method too if a proper attention was paid for the consistency between the numerical and analytical differentiation. With use of the "consistent" finite difference scheme, Kawamura and Kondoh (1996) performed the DNS of the turbulent channel flow for $Pr = 0.71$ and $Re_\tau = 180$ and obtained a good agreement with the one by the spectral method. Further comparisons with the spectral method by Kasagi et al. (1992) will be presented also in the present paper to confirm the validity of the adopted numerical method.

In the present work, DNS of the turbulent heat transfer for various Prandtl numbers ranging from 0.025 to 5 are performed with the finite difference method to obtain turbulence quantities such as turbulent heat flux, temperature variance, their budget terms and the turbulent Prandtl number. The data for the intermediate Prandtl numbers such as $Pr = 0.1$, 0.2, 0.4 are rather difficult to be obtained experimentally. The Prandtl number of 5 is, to the author's knowledge, the highest value ever calculated for the turbulent heat transfer of a channel flow.

It is known that the smallest scale in the temperature fluctuation decreases with the increase of the Prandtl number inversely proportional to $Pr^{1/2}$ (Tennekes and Lumley, 1972). Thus, in the calculation of $Pr = 5$ the mesh number is doubled in each direction. This causes roughly ten times calculation cost, which is the reason why the DNS for this range of the Prandtl number has not been made hitherto. The present calculation has been enabled by means of a super parallel computer "Numerical Wind Tunnel (NWT)" using about eight million mesh points and 1 GB main memory.

2. Numerical procedure

The configuration is the fully developed channel flow (Fig. 1). The computational domain is 6.4δ, 2δ, 3.2δ in the axial, wall-normal, and spanwise directions, respectively. The mean flow is in x direction. The flow is heated with a uniform heat flux from both the walls. The distance, instantaneous velocity, temperature and pressure are nondimensionalized by the channel half width, friction velocity, the kinematic viscosity, the density and the friction temperature.

The fundamental equations are:

Continuity equation

$$\frac{\partial \tilde{U}_i^+}{\partial x_i^*} = 0, \tag{1}$$

Navier–Stokes equation

$$\frac{\partial \tilde{U}_i^+}{\partial t^+} + \tilde{U}_j^+ \frac{\partial \tilde{U}_i^+}{\partial x_j^*} = -\frac{\partial \tilde{P}^+}{\partial x_i^*} + \frac{1}{Re_\tau} \frac{\partial^2 \tilde{U}_i^+}{\partial x_j^{*2}}. \tag{2}$$

In this case, the statistically averaged temperature increases linearly with respect to x. Then the instantaneous temperature $\tilde{T}^+(x, y, z)$ can be divided into two parts

$$\tilde{T}^+(x^*, y^*, z^*) = \frac{\mathrm{d}\langle T_m^+ \rangle}{\mathrm{d}x^*} x^* - \tilde{\Theta}^+(x^*, y^*, z^*), \tag{3}$$

where $\langle T_m^+ \rangle$ is the so-called mixed mean temperature defined as

$$\langle T_m^+ \rangle = \int_0^1 U_1^+ T^+ \, \mathrm{d}y^* \Big/ \int_0^1 U_1^+ \, \mathrm{d}y^*. \tag{4}$$

In the present configuration, its streamwise gradient becomes

$$\frac{\mathrm{d}\langle T_m^+ \rangle}{\mathrm{d}x^*} = 1/\langle U^+ \rangle, \tag{5}$$

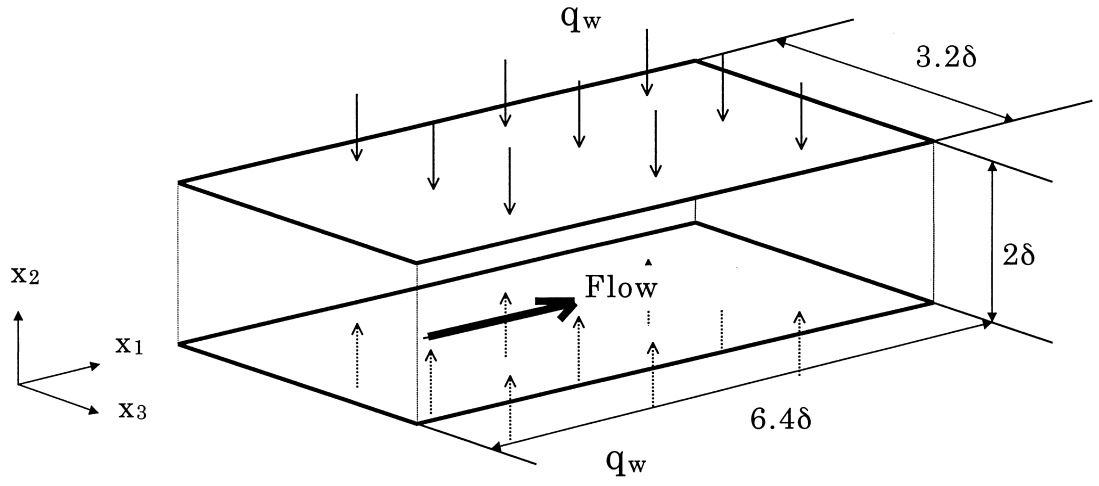

Fig. 1. Configuration of DNS.

Table 1
Computational conditions

Reynolds number	$\mathrm{Re}_\tau = 180$
Mesh	Staggered mesh
Coupling algorithm	Fractional step method
Time advancement	2nd-order Adams–Bashforth method
Convective term	2nd central (consistent scheme)
Other terms	2nd central
Boundary conditions	Periodic (x, z direction) Non-slip (y direction)
Computational volume	$6.4\,\delta \times 2\,\delta \times 3.2\,\delta$
Grid number	$128 \times 66 \times 128$ ($\mathrm{Pr} \leqslant 1.5$) $256 \times 128 \times 256$ ($\mathrm{Pr} = 5.0$)

where $\langle U^+ \rangle$ is the average velocity over the channel section. With the above transform, the energy equation becomes

$$\frac{\partial \tilde{\Theta}^+}{\partial t^+} + \tilde{U}_j^+ \frac{\partial \tilde{\Theta}^+}{\partial x_j^*} = \frac{1}{\mathrm{Re}_\tau \cdot \mathrm{Pr}} \frac{\partial^2 \tilde{\Theta}^+}{\partial x_j^{*2}} + \frac{\tilde{U}_1^+}{\langle U^+ \rangle}. \tag{6}$$

The boundary conditions are

$$\tilde{U}_i^+ = 0, \quad \tilde{\Theta}^+ = 0 \text{ at } y = 0, 2\delta. \tag{7}$$

The above equations are discretized with the use of the finite difference method. A numerical scheme consistent with the analytical operation (Kawamura, 1995) is employed to ensure the balance of the transport equations for the statistical correlations such as the turbulent heat flux and the temperature variance. The computational conditions are given in Table 1.

3. Results

The mean temperature profile is given in Fig. 2 for various Prandtl numbers. The results agree well with the Kader's correlation (Kader, 1981). The mean temperature profile is plotted again in Fig. 3 with an emphasis on the conduction region. It is well known that the near-wall temperature variation can be expanded in terms of y^+ as

$$\Theta^+ = \mathrm{Pr}\, y^+ + \cdots \tag{8}$$

which is clearly shown in Fig. 3. This figure further indicates that the conduction region penetrates more deeply into the core region with decrease of the Prandtl number. The results by Kasagi et al. (1992) with $\mathrm{Pr} = 0.71$ are plotted for comparison in Fig. 3 and in some of the following figures. The present results agree quite well with them except for the central region, where a slight discrepancy arises because of the difference in Re_τ.

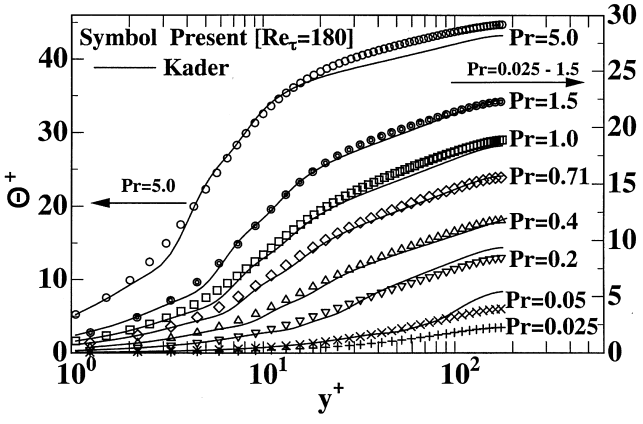

Fig. 2. Mean temperature profile with an emphasis on the logarithmic region.

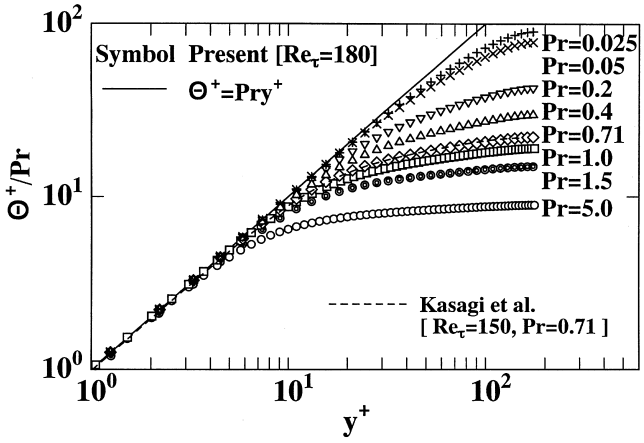

Fig. 3. Mean temperature profile with an emphasis on the conduction region.

The Nusselt number is nondimensionalized in the present definitions as

$$\mathrm{Nu} = \frac{2\delta\alpha}{\lambda} = 2\mathrm{Re}_\tau\, \mathrm{Pr}/\langle \Theta_m^+ \rangle. \tag{9}$$

The obtained Nusselt number is shown as a function of the Prandtl number in Fig. 4. The results are compared with the empirical correlation by Sleicher and Rouse (1975). The correlation is originally for the circular tube; moreover, the present Re_m of 5600 is smaller than the applicable range of the correlation. Nevertheless, both agree satisfactorily well for the wide range of the calculated Prandtl numbers.

Since the fully developed condition is assumed in this simulation the mean temperature Θ^+ is governed by the following energy equation

$$\frac{\mathrm{d}}{\mathrm{d}y^+}\left[\frac{1}{\mathrm{Pr}}\frac{\mathrm{d}\Theta^+}{\mathrm{d}y^+} - \overline{v^+\theta^+}\right] = -\frac{1}{\mathrm{Re}_\tau}\frac{U_1^+}{\langle U^+ \rangle}. \tag{10}$$

The total heat flux, that is the sum of the molecular and turbulent heat fluxes, can be obtained by integrating Eq. (10) from $y^+ = 0$ to y^+ as

$$q_{\mathrm{total}}^+ = \frac{1}{\mathrm{Pr}}\frac{\mathrm{d}\Theta}{\mathrm{d}y^+} - \overline{v^+\theta^+} = 1 - \frac{1}{\mathrm{Re}_\tau}\int_0^{y^+} \frac{U_1^+}{\langle U^+ \rangle}\mathrm{d}y^+. \tag{11}$$

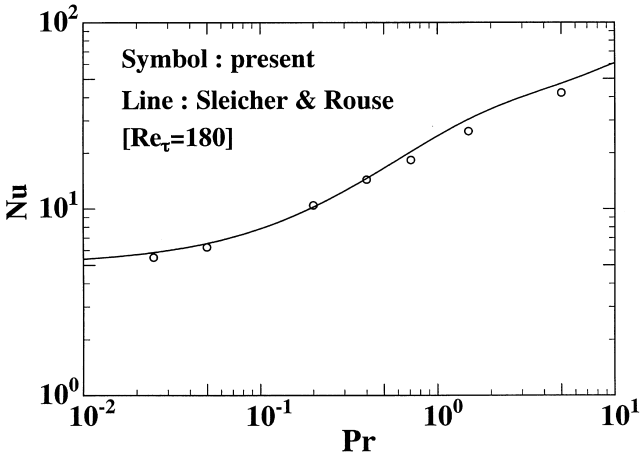

Fig. 4. Relation between Nusselt and Reynolds numbers.

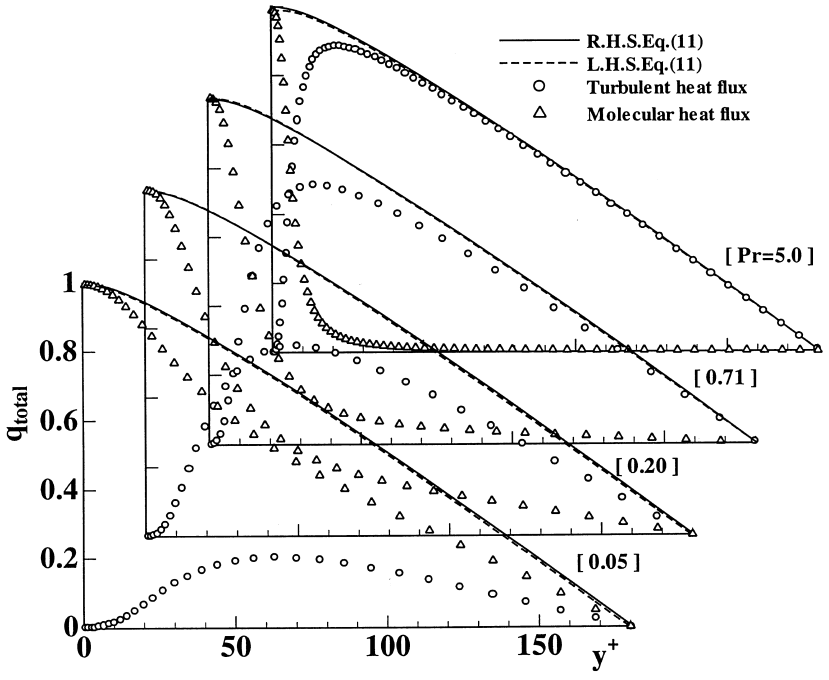

Fig. 5. Turbulent and molecular heat fluxes.

The above equality is examined and the results are shown in Fig. 5. The agreement between both sides of Eq. (11) is almost good. The small discrepancy found in Fig. 5 can be regarded as a measure of the computational uncertainty. Fig. 5 indicates that the wall-normal turbulent heat flux increases with the increase of the Prandtl number, which is balanced by the decrease in the molecular heat flux.

In the wall vicinity, the fluctuations of the velocity and temperature can be expanded in terms of y^+ as

$$u^+ = b_1 y^+ + c_1 y^{+^2} + \cdots, \tag{12}$$

$$v^+ = c_2 y^{+^2} + d_2 y^{+^3} + \cdots, \tag{13}$$

$$w^+ = b_3 y^+ + c_3 y^{+^2} + \cdots. \tag{14}$$

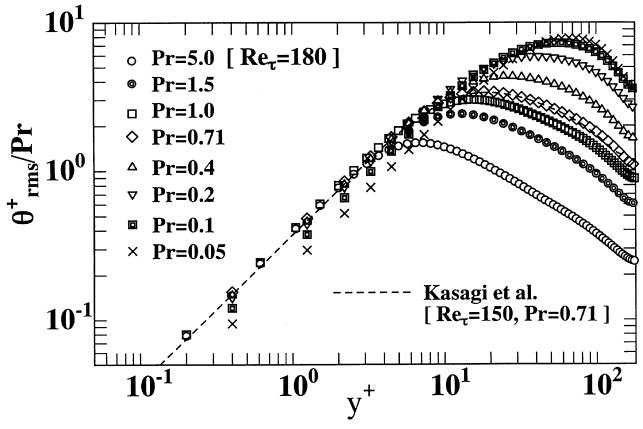

Fig. 6. The root mean square of temperature variance.

On the other hand, the gradient of the instantaneous temperature $\tilde{\Theta}^+$ over the heating boundary satisfies the relation

$$\frac{1}{\mathrm{Pr}}\frac{\mathrm{d}\tilde{\Theta}^+}{\mathrm{d}y^+} = 1 + \frac{q'_w}{\overline{q}_w}, \quad y = 0, \tag{15}$$

where $\overline{q}_w$ is the average heat flux and q'_w is its fluctuation. If Eq. (15) is decomposed into the mean and fluctuating parts and Eq. (8) is considered, the fluctuation temperature satisfies the following equation

$$\frac{1}{\mathrm{Pr}}\frac{\mathrm{d}\theta^+}{\mathrm{d}y^+} = \frac{q'_w}{\overline{q}_w}. \tag{16}$$

This indicates that θ^+ may be expanded as

$$\theta^+ = \mathrm{Pr}(b_\theta y^+ + c_\theta y^{+^2} + \cdots). \tag{17}$$

The coefficient b_θ can still be a function of the Prandtl number. In case of an extremely highly conductive fluid, for example, the fluctuation q'_w will strongly tend to zero. So, one may expect that b_θ decreases for a very low Prandtl number fluid.

The root mean square of the temperature variance divided by Pr is shown in Fig. 6, which indicates that the coefficient b_θ in Eq. (17) is mostly constant ($b_\theta \sim 0.38$) for a wide range of Pr. For a low Prandtl number of $\mathrm{Pr} < 0.1$, b_θ decreases as discussed above.

With the use of Eqs. (12), (13) and (17), the turbulent heat fluxes are expressed as:

$$\overline{u^+\theta^+} = \mathrm{Pr}(\overline{b_1 b_\theta} y^{+^2} + \overline{c_1 b_\theta} y^{+^3} + \cdots), \tag{18}$$

$$-\overline{v^+\theta^+} = \mathrm{Pr}(\overline{b_\theta c_2} y^{+^3} + \overline{b_\theta d_2} y^{+^4} + \cdots). \tag{19}$$

Thus one can expect that in the wall vicinity $\overline{u^+\theta^+}/\mathrm{Pr}$ and $-\overline{v^+\theta^+}/\mathrm{Pr}$ vary as y^{+2} and y^{+3} respectively. Indeed Figs. 7 and 8 confirm the above relation with their correlation coefficients

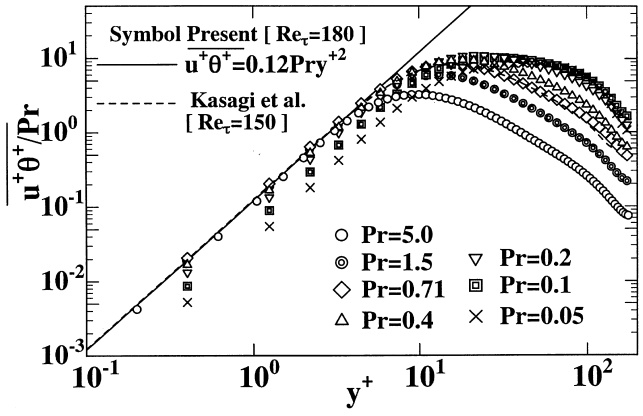

Fig. 7. Streamwise turbulent heat flux.

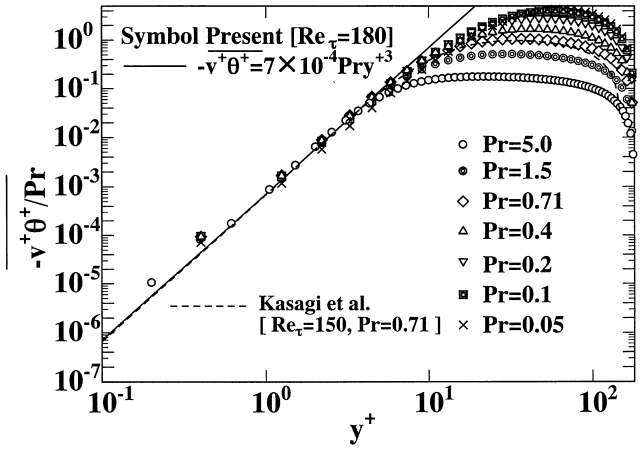

Fig. 8. Wall-normal turbulent heat flux.

$\overline{b_1 b_\theta} = 0.12$ and $\overline{b_\theta c_2} = 7 \times 10^{-4}$, which are in good agreement with the ones obtained by Antonia and Kim (1991). Both coefficients are mostly independent of Pr for Pr > 0.2, while $\overline{b_\theta c_2}$ decreases for Pr < 0.1 as b_θ itself does.

The turbulent Prandtl number ($\mathrm{Pr_t}$) is an important and useful quantity for practiced heat transfer calculations. It is often assumed to be constant irrespectively of the wall-normal distance and the molecular Prandtl number atleast for Pr ⩾ 1. Its dependence on the distance and Pr has long been a subject of many investigations. Kays (1994) proposed a correlation for $\mathrm{Pr_t}$ referring several independent experiments. It showed rather steep increase as the wall was approached. In the turbulence modelling, Nagano et al. (1993) proposed a turbulence model which predicted an increasing $\mathrm{Pr_t}$ with increase of Pr.

The turbulent Prandtl number is defined as

$$\mathrm{Pr_t} = \frac{\nu_t}{a_t} = \frac{\overline{u^+v^+}\,(\mathrm{d}\Theta^+/\mathrm{d}y^+)}{\overline{v^+\theta^+}\,(\mathrm{d}U_1^+/\mathrm{d}y^+)}. \tag{20}$$

With the use of Eqs. (8), (12), (13) and (19), one finds that

$$\mathrm{Pr_t} = \frac{\overline{b_1 c_2}}{\mathrm{Pr}\overline{b_\theta c_2}}\frac{\mathrm{Pr}}{1} = \frac{\overline{b_1 c_2}}{\overline{b_\theta c_2}}, \quad (y^+ \to 0). \tag{21}$$

Since $\overline{b_1 c_2} \approx 7 \times 10^{-4}$ (Mansour et al., 1988), $\mathrm{Pr_t}$ tends to be about 1.0 as the wall is approached. Moreover the above consideration indicates that the wall asymptotic value of the turbulent Prandtl number is also independent of the molecular Prandtl number at least for Pr ⩾ 0.2.

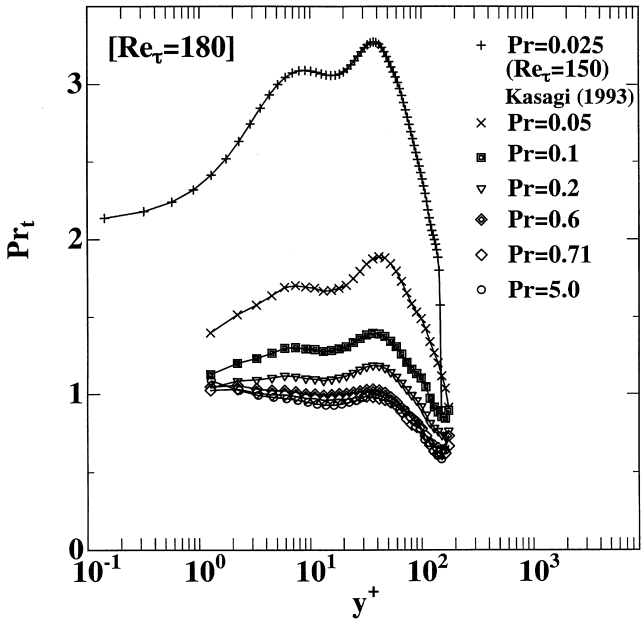

Fig. 9. Turbulent Prandtl number.

The turbulent Prandtl numbers obtained through the present DNS are shown in Fig. 9. Indeed, the wall asymptotic value of Pr is independent of Prandtl number except for very low Prandtl numbers such as Pr < 0.1. This feature was suggested by Antonia and Kim (1991) up to Pr = 2; and it is extended here to a higher Prandtl number. Moreover, for the higher Pr, the present author (Kawamura, 1996) showed analytically that, in the wall vicinity, $\mathrm{Pr_t}$ is independent of both Pr and y based on the well accepted relation of Nu ∝ $\mathrm{Pr}^{1/3}$ for Pr≫1. Thus, one can conclude that the turbulent Prandtl number does not dependent upon the wall-normal distance and the molecular Prandtl number for normal to high Prandtl number fluids. This conclusion supports the widely used practice to employ a constant turbulent Prandtl number in the calculation of heat transfer.

The turbulence energy k, the temperature variance $\overline{\theta^2}$ and their dissipations construct a nondimensional quantity called as the time constant ratio

$$R = \frac{\overline{\theta^2}\varepsilon}{2k\varepsilon_\theta}. \tag{22}$$

It is also an important quantity because the dissipation of the temperature variance ε_θ is often calculated with an assumption of a constant R. The wall a symptotic form of these quantities are:

$$k = \frac{1}{2}\overline{u_i^2} \to \frac{1}{2}(\overline{b_1^2} + \overline{b_3^2})\,y^2, \tag{23}$$

$$\varepsilon = \nu\overline{\left(\frac{\partial u_i}{\partial x_j}\right)^2} \to \nu(\overline{b_1^2} + \overline{b_3^2}), \tag{24}$$

$$\overline{\theta^2} \to \overline{b_\theta^2}y^2, \tag{25}$$

$$\varepsilon_\theta = a\overline{\left(\frac{\partial \theta}{\partial x_j}\right)^2} \to a\overline{b_\theta^2}. \tag{26}$$

Thus R tends exactly to Pr as the wall is approached. The time constant ratio is shown in Fig. 10 for various Prandtl

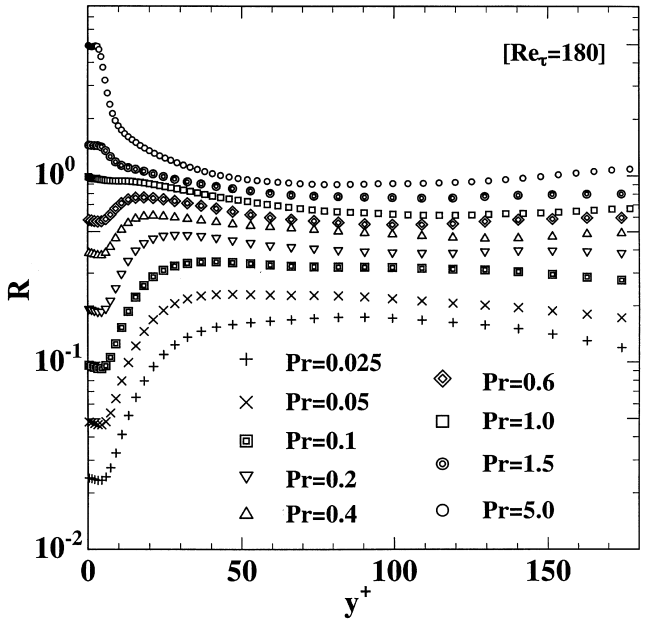

Fig. 10. Time constant ratio.

numbers. Its wall limiting value is certainly equal to the Prandtl number. In the central region, R becomes closer to the unity. More detailed inspection indicates that, for $\mathrm{Pr}=0.7$, R is about 0.5, which is a value often assumed by the simplified heat transfer calculation. It becomes approximately unity when $\mathrm{Pr}=5$.

The budget of the transport equation for the turbulent heat flux is given in Fig. 11(a)–(d). The production term is negative in this case. It is well known that, in case of the fluid with $\mathrm{Pr}\geqslant 0.7$, the dissipation

$$\varepsilon_{i\theta}=(a+v)\overline{\frac{\partial u_i}{\partial x_j}\frac{\partial \theta}{\partial x_j}} \tag{27}$$

is negligible because of the isotropy in the dissipation scale. It is actually seen that the dissipation is negligibly small for $\mathrm{Pr}=5.0$ (Fig. 11(d)) except in the wall vicinity. Thus, the production is balanced by the temperature–pressure -gradient correlation (TPG) term

$$\phi_{i\theta}=-\overline{\theta\frac{\partial p}{\partial x_i}}. \tag{28}$$

In a low Prandtl number fluid, on the other hand, the dissipation is dominant because it takes place in eddies of a larger scale (see Fig. 11(a)). Indeed, Fig. 11(c) and (d) show that the TPG term is dominant for $\mathrm{Pr}=0.4$ and 5.0 while the dissipation term is overwhelming for $\mathrm{Pr}=0.05$. It is interesting to note that the TPG and the dissipation terms become comparative at $\mathrm{Pr}=0.2$ as seen in Fig. 11(b).

The instantaneous contour surfaces of the budget terms on the transport equation for the wall normal heat flux are visualized for $\mathrm{Pr}=0.05$ and 5.0 in Fig. 12(a) and (b), respectively. As discussed above, the dissipation overcomes the TPG for $\mathrm{Pr}=0.05$. On the other hand, in the high Prandtl

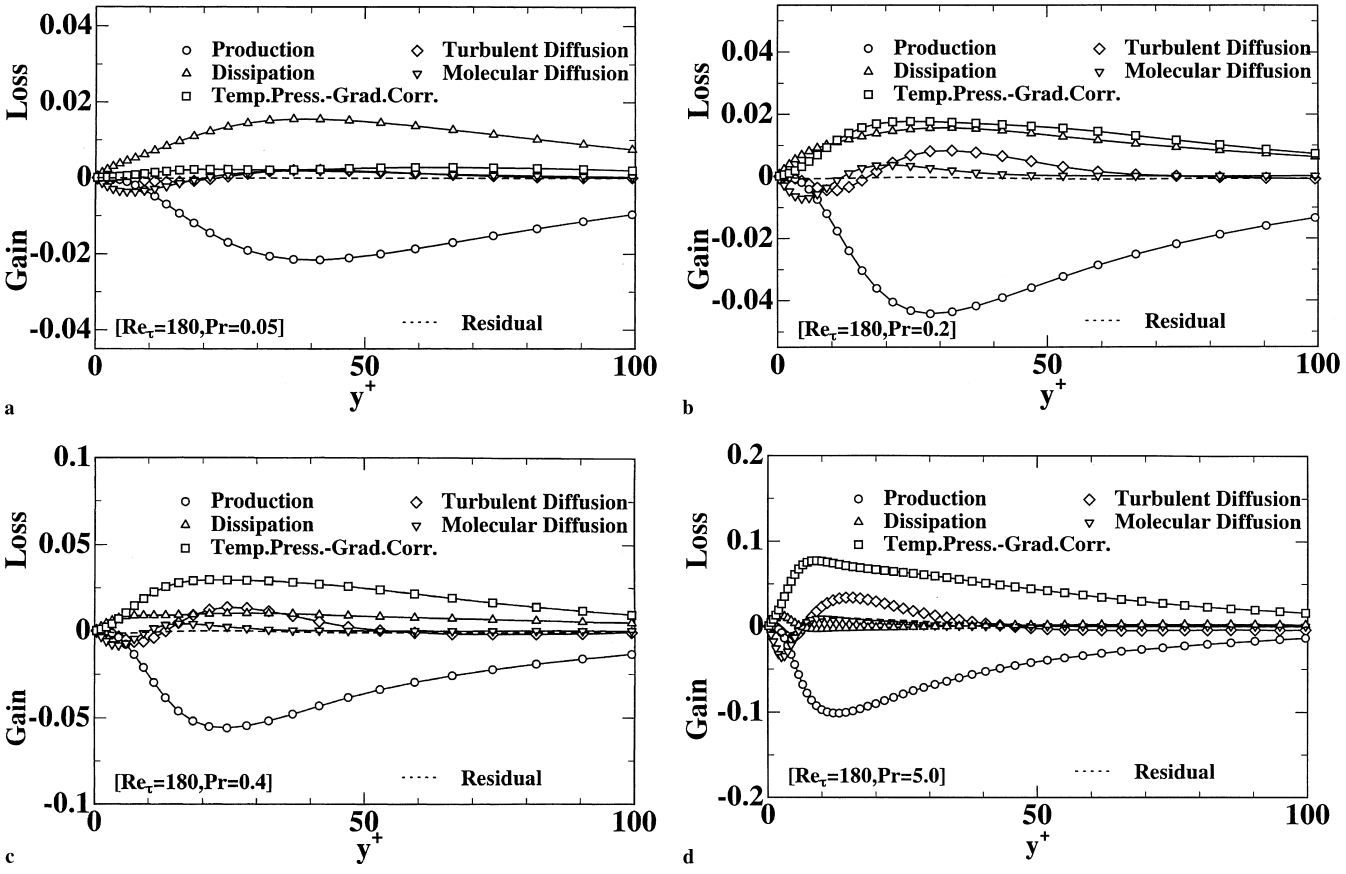

Fig. 11. Budget of the transport equation for the wall-normal turbulent heat flux: (a) $\mathrm{Pr}=0.05$, (b) $\mathrm{Pr}=0.2$, (c) $\mathrm{Pr}=0.4$, (d) $\mathrm{Pr}=5.0$.

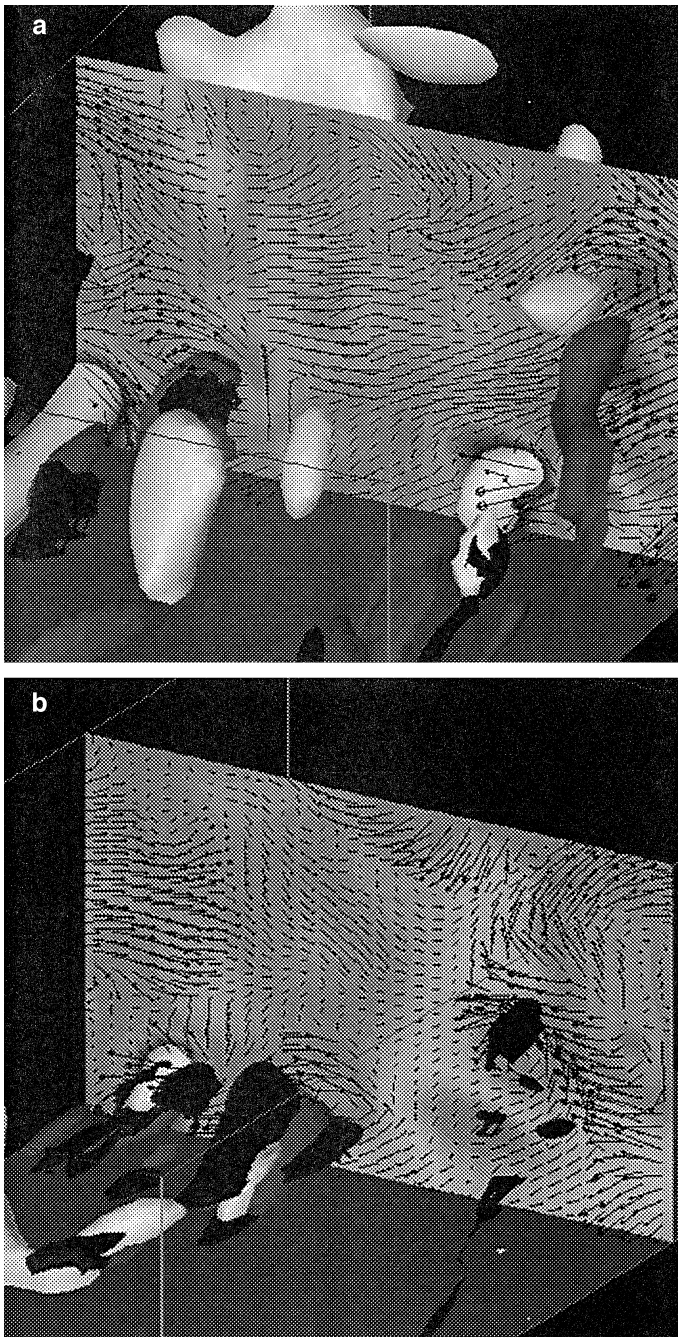

Fig. 12. Velocity vector and contour surfaces of budget terms in the transport equation of $\overline{v^+\theta^+}$: (a) $Pr = 0.05$, (b) $Pr = 5.0$; white:low pressure region, gray:dissipation, black:TPG; span $z^+ = 288$, height $y^+ = 180$.

number of $Pr = 5.0$, the TPG dominates and the dissipation is hardly visible. Moreover, the structure of the TPG is seen to become elongated in the streamwise direction and more slender in the spanwise direction with the increase of the Prandtl number.

The instantaneous dissipation terms of $Pr = 0.05$ and 5 are compared in Fig. 13(a) and (b). It is interesting to note that in case of $Pr = 0.05$, only the positive value appears while in $Pr = 5.0$ both positive and negative values appear to compensate each other resulting a negligible contribution in the budget of the transport equation. With notice of this point, the distribution of the ensemble averaged dissipation for the wall normal heat flux is reexamined. The result is shown in Fig. 14. It is appended to emphasise the negativity of $\varepsilon_{2\theta}$ at $Pr = 5.0$. It is interesting to note that, at the highest Pr of 5.0, the dissipation term becomes even negative, i.e. contributes as "gain", in some of the near wall region.

The temperature variance is illustrated in Fig. 15 for various Prandtl numbers. The peak of the temperature variance becomes higher and moves closer to a wall as the Prandtl number increases.

The budget terms of the transport equation of the temperature variance are given in Fig. 16(a)–(c). The production term is mostly balanced with the dissipation for all Prandtl

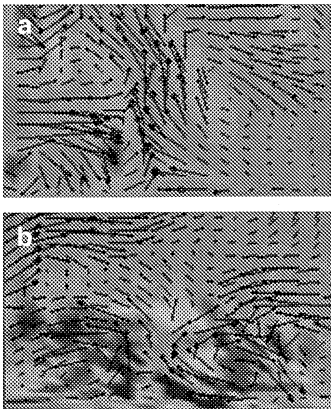

Fig. 13. Contour of dissipation in the transport equation of $\overline{v^+\theta^+}$: (a) $Pr = 0.05$, (b) $Pr = 5.0$; gray to black:positive (loss); gray to white:negative (gain); span $z^+ = 144$, height $y^+ = 90$.

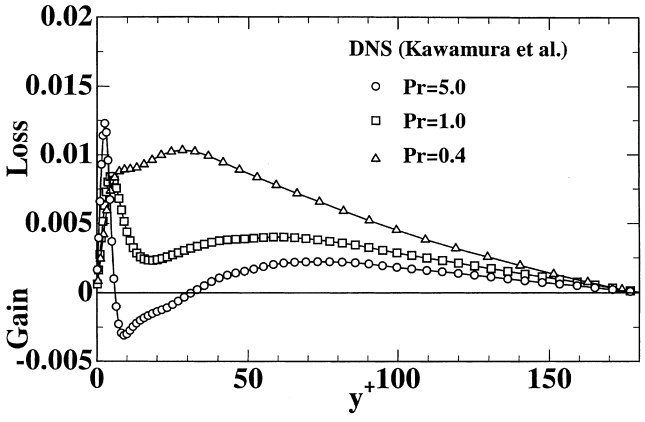

Fig. 14. Dissipation of wall-normal heat flux for various Prandtl numbers.

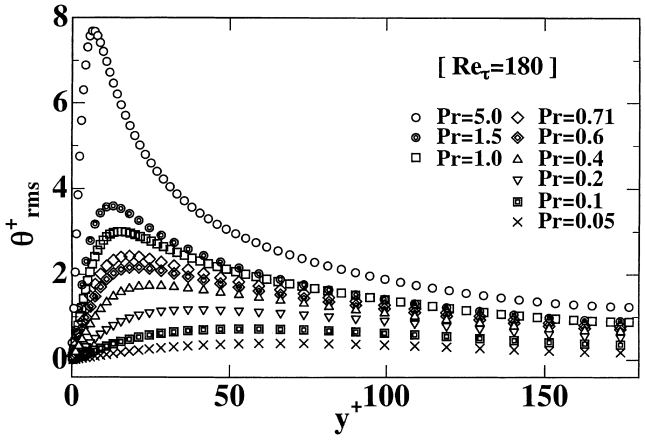

Fig. 15. Temperature variance for various Prandtl numbers.

number calculated. A closer inspection, however, indicates that the turbulent and molecular diffusion terms play a more significant role with increase of the Prandtl number. In case of $Pr = 5.0$, the diffusion terms become even comparative with the dissipation, which has never been seen in the lower Prandtl number cases.

It is seen in Fig. 16(a)–(c) that the peak in the production term increases and moves towards the wall with increasing Prandtl number. The ensemble averaged energy equation for the fully developed flow is given by Eq. (11). Since $\overline{u^+} = y^+$ in the wall vicinity, Eq. (11) can be integrated with respect to y^+ as

$$\frac{1}{\mathrm{Pr}}\frac{\mathrm{d}\Theta^+}{\mathrm{d}y^+} = 1 - \left(-\overline{v^+\theta^+}\right) - \frac{1}{2\mathrm{Re}_m}y^{+2}. \tag{29}$$

The last term in the right-hand side is negligible compared to the other terms. Then the production term of the temperature variance can be expressed simply as

$$P_\theta = -\overline{v^+\theta^+}\frac{\mathrm{d}\Theta^+}{\mathrm{d}y^+} = \mathrm{Pr}\left(-\overline{v^+\theta^+}\right)\left[1 - \left(-\overline{v^+\theta^+}\right)\right]. \tag{30}$$

It is easily found that the maximum in P_θ arises at $-\overline{v^+\theta^+} = 0.5$ with its peak value of

$$P_{\theta\max} = \mathrm{Pr}/4, \quad (\mathrm{Pr} \gg 1.0) \tag{31}$$

as already noted by Teitel and Antonia (1993). If only the first term in Eq. (19) is adopted for simplicity, the position of peak can be approximated as

$$y^+_{\max} = \frac{1}{2\left(b_\theta c_2\right)^{1/3}}\frac{1}{\mathrm{Pr}^{1/3}}, \quad (\mathrm{Pr} \gg 1.0). \tag{32}$$

Thus, P_θ/Pr is plotted versus $\mathrm{Pr}^{1/3}\ y^+$ in Fig. 17. It is found that, except for low Prandtl numbers such as $Pr < 0.1$, the peak and its position can be well normalized with the above treatment.

Finally, it should be mentioned that the present DNS has been performed with a relatively low Reynolds number of $\mathrm{Re}_\tau = 180$. Antonia et al. (1992) and Antonia and Kim (1994) analyzed the effect of Reynolds number on the Reynolds stress and other turbulent statistical quantities. They found that increase of Re_τ caused nonneglible change in those quantities although their fundamental feature was unchanged. The same trend can be anticipated for the scalar transportation, too. The present authors' group is now performing the DNS of turbulent scalar transport with a higher Reynolds number, which will be reported in near future.

4. Conclusions

1. DNS of the turbulent heat transfer in channel flow was performed for more than two decades of the Prandtl number from 0.025 to 5; the largest one ($Pr = 5$) is, to the author's knowledge, the highest Prandtl number calculated to date.
2. The budget terms of the transport equations for the turbulent heat flux and the temperature variance were obtained and visualized. The effect of the Prandtl number was examined.
3. The near wall behavior of the turbulent quantities were analyzed and statistical correlation coefficients were obtained for the above range of Pr.
4. The wall limiting value of the distance from the wall and the turbulent Prandtl number was proved to be independent of the molecular Prandtl number except for a low Prandtl number fluid. This conclusion gives a theoretical basis on the widely employed practice to use a constant Pr_t in the heat transfer calculation of the fluids with the normal to high molecular Prandtl number.

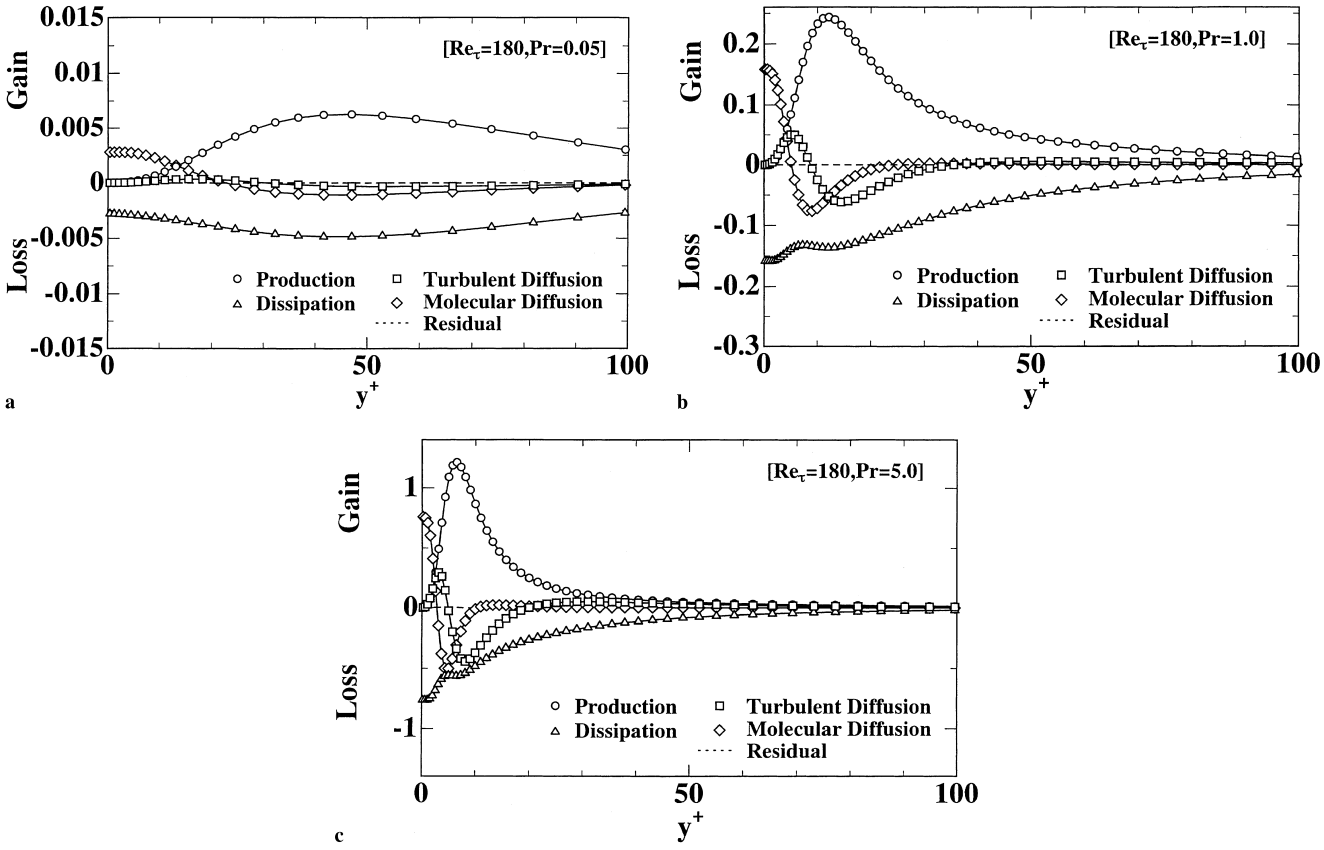

Fig. 16. Budget of the transport equation for the temperature variance: (a) Pr = 0.05, (b) Pr = 1.0, (c) Pr = 5.0.

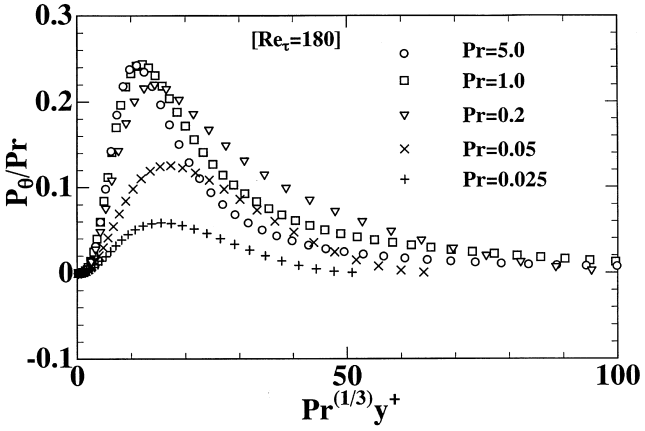

Fig. 17. Normalized profile of production term of the temperature variance.

The present data base is open to public access. The detailed information is given at http://muraibm.me.noda.sut.ac.jp/e-page1.html.

References

Antonia, R.A., Kim, J., 1991. Turbulent Prandtl number in the near-wall region of a turbulent channel flow. Int. J. Heat Mass transfer 34, 1905–1908.

Antonia, R.A. et al., 1992. Low-Reynolds number effects in a fully developed turbulent channel flow. J. Fluid Mech 236, 597–605.

Antonia, R.A., Kim, J., 1994. Low-Reynolds number effects on near turbulence. J. Fluid Mech. 276, 61–80.

Kader, B.A., 1981. Temperature and concentration profiles in fully turbulent boundary layers. Int. J. Heat Mass Transfer 24, 1541–1544.

Kasagi, N., Tomita, Y., Kuroda, A., 1992. Direct numerical simulation of passive scalar field in a turbulent channel flow. ASME J. Heat Transfer 144, 598–606.

Kasagi, N., Ohtsubo, Y., 1993. Direct Numerical Simulation of Low Prandtl Number Thermal Field in a Turbulent Channel Flow. In: Turbulent Shear Flows, vol. 8, Springer, Berlin, pp. 97–119.

Kawamura, H., 1995. Direct Numerical Simulation of Turbulence by Finite Difference Scheme. In: The Recent Developments in Turbulence Research. International Academic Publishers, pp. 54–60.

Kawamura, H., 1996. Turbulence Modelling. In: Yohkendo, (Ed.), Progress in Heat transfer, New series 2. JSME pp. 51–56 (in Japanese).

Kawamura, H., Kondoh, Y., 1996. Application of Consistent Finite Difference Scheme to DNS of Turbulent Heat Transfer in Channel Flow. In: Proceedings of the Third KSME-JSME Thermal Engineering Conference, vol. 1, pp. 53–58.

Kays, W.M., 1994. Turbulent Prandtl Number – Where Are We? Trans. ASME J. Heat Transf. 116, 284–295.

Kim, J., Moin, P., 1989. Transport of Passive Scalars in a Turbulent Channel Flow. In: Turbulent Shear Flows, vol. 6, Springer, Berlin, pp. 85–96.

Lyons, S.L., Hanratty, T.J., Mclaughlin, J.B., 1991. Direct numerical simulation of passive heat transfer in a turbulent channel flow. Int. J. Heat Mass Transfer 34, 1149–1161.

Mansour, N., Kim, J., Moin, P., 1988. Reynolds-stress and dissipation-rate budgets in a turbulent channel flow. J. Fluid Mech. 194, 15–44.

Nagano, Y. et al., 1993. Numerical analysis of turbulent heat transfer in various Prandtl number fluids. In: Proceedings of the Fifth International Symposium on Computational Fluid Dynamics, II.

Sleicher, C.A., Rouse, M.W., 1975. A convenient correlation for heat transfer to constant and variable property fluids in turbulent pipe flow. Int. J. Heat Mass Transfer 18, 677–683.

Teitel, M., Antonia, R.A., 1993. Heat transfer in fully developed turbulent channel flow: Comparison between experiment and direct numerical simulations. Int. J. Heat Mass transfer 36, 1701–1706.

Tennekes, H., Lumley, J.L., 1972. In: A First Course in Turbulence, MIT Press, Cambridge, MA, pp. 96–97.